ACS APPLIED MATERIALS & INTERFACES

Research Article

Cite This: ACS Appl. Mater. Interfaces 2019, 11, 21915−21925

www.acsami.org

Photochemically Enhanced Selective Adsorption of Gold Ions on Tannin-Coated Porous Polymer Microspheres

Jeonga Kim,[†] Kyeong Rak Kim,[†] Yeongran Hong,[‡] Sunyoung Choi,[§] Cafer T. Yavuz,[‡,∥,⊥] Jin Woong Kim,[*,#,■] and Yoon Sung Nam[*,†,●]

[†]Department of Materials Science and Engineering, [‡]Graduate School of Energy, Environment, Water and Sustainability (EEWS), [∥]Department of Chemical and Biomolecular Engineering, [⊥]Department of Chemistry, and [●]KAIST Institute for NanoCentury, Korea Advanced Institute of Science and Technology, 291 Daehak-ro, Yuseong-gu, Daejeon 34141, Republic of Korea

[§]CTK Cosmetics, 255 Pangyo-ro, Seongnam-si, Gyeonggi-do 13486, Republic of Korea

[#]Department of Bionano Technology and [■]Department of Chemical and Molecular Engineering, Hanyang University, Ansan 15588, Republic of Korea

S *Supporting Information*

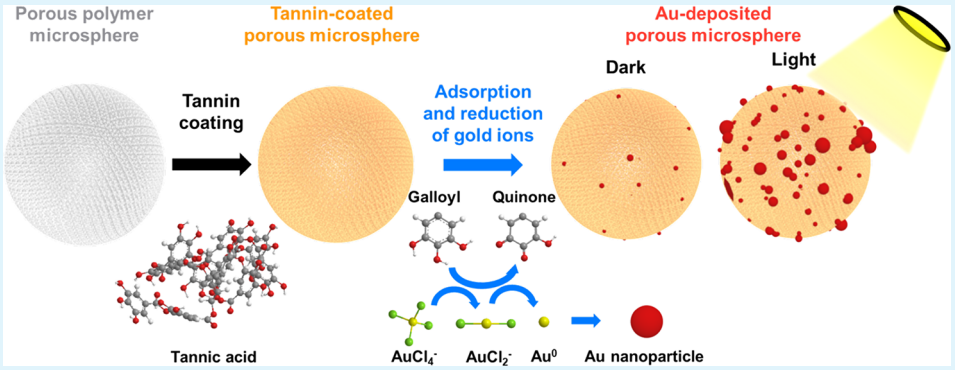

ABSTRACT: Metal recovery from electronic waste and industrial wastewater has attracted increasing attention to recycle precious metals and inhibit the emission of hazardous heavy metals. However, the selective recovery of precious metals with a large quantity is still very challenging because wastewater contains a variety of different cations while precious metal ions are relatively scarce. Here, we introduce a simple method to selectively increase the adsorption of gold ions using tannin-coated porous polymer microspheres through photochemical reduction. Mesoporous poly(ethylene glycol dimethacrylate-*co*-acrylonitrile) microspheres with an average pore diameter of 13.8 nm were synthesized and used as an adsorbent matrix. Tannic acid (TA) was deposited onto the internal pores of the polymer matrix by simple immersion in an aqueous milieu. TA coatings increased the maximum number of adsorbed gold ions by 1.3 times because of the well-known metal ion chelation of TA. Under light illumination, the maximum number of adsorbed gold ions dramatically increased by 6.1 times. We examined two distinct mechanisms presumably involved in the enhanced adsorption: the photooxidation of TA and plasmon-induced hot electrons. Moreover, TA-coated microspheres exhibited remarkable selectivity for gold ions among competing metal ions commonly found in waste resources. This work suggests that the photochemically activated TA can serve as an excellent adsorbent for the selective and efficient recovery of gold ions from wastewater.

KEYWORDS: *metal recovery, gold adsorption, photochemistry, tannic acid, selectivity*

1. INTRODUCTION

The recovery of precious metals (e.g., Au, Ag, Pt, and Pd) has received increasing attention as a concept of "urban mining", which means the recovery of raw materials from the electronic waste of the city.[1] Urban mining is considered more efficient than natural mining because waste resources have a larger amount of precious metals than ores, especially in printed circuit boards, and the emission of them is gradually rising because of the increasing consumption of electronic devices.[1,2] However, the selective recovery of precious metals remains technically very challenging because electronic wastes contain very diluted precious metal ions with a variety of metal ions and other cations being present.

Among precious metals, gold has been widely utilized for electronics because of its outstanding electrical conductivity and chemical stability against corrosion. The recovery of gold has been investigated by various techniques, including hydrometallurgical and pyrometallurgical processes, such as

Received: March 23, 2019
Accepted: May 28, 2019
Published: June 10, 2019

Downloaded via KING ABDULLAH UNIV SCI TECHLGY on February 9, 2022 at 08:10:49 (UTC).
See https://pubs.acs.org/sharingguidelines for options on how to legitimately share published articles.

© 2019 American Chemical Society

DOI: 10.1021/acsami.9b05197
ACS Appl. Mater. Interfaces 2019, 11, 21915−21925

cementation (also called chemical precipitation or coagulation), adsorption, ion exchange, solvent extraction, and electrowinning.[3] The hydrometallurgical process employs leaching agents to extract gold ions from solid waste resources. This process is currently preferred because of better accuracy and predictability, easier controllability, and more comfortable operation.[4] However, the existing hydrometallurgical process is very expensive, labor-intensive, and time-consuming because of the many requirements of reagents and energy. Also, it is not environmentally friendly because of the production of waste products and incomplete metal removal.[4,5] Among the methods mentioned above, adsorption is considered environmentally friendly, inexpensive, and easy for handling. It is also suitable for the solution of very diluted metal ions, which is very common to wastewater.[6] Multiple absorbents have been explored for gold recovery, including activated carbons and bioadsorbents (e.g., fungi, algae, bacteria, and chitosan), and surface modification of substrates with functional groups (e.g., amines, thiols, cyanide, and amidoxime) has been attempted.[3,7−9] However, their selectivity to gold ions, that is, the competitive adsorption of gold ions among other abundant metal ions, and the underlying mechanisms have not yet been well studied.

Bioinspired adhesive materials have been extensively investigated to produce multifunctional coating layers for the surface modification of various substrates.[10−14] Many bioinspired adhesive materials contain polyphenols (e.g., catechol or galloyl moieties) as found in natural adhesive molecules.[15−18] Polyphenols can easily produce excellent coating layers at a low cost and form coordination complexes with various metal ions.[19] Polyphenols can also serve as an excellent reducing agent for metal ions to generate various metal nanostructures of precious metals (e.g., Au, Ag, and Pd).[20−24] Tannic acid (TA), one of the plant polyphenols and a commercial form of tannin, consists of glucose with five hydroxyl groups combined with digallic acid, resulting in a large number of phenolic hydroxyl groups to help efficiently form bonds with multiple metal ions.[25]

Previous studies showed that gold ions can be adsorbed and reduced by phenolic hydroxyl groups.[26−28] TA has a standard redox potential of 0.897 V versus normal hydrogen electrode (NHE). This mild reduction power is a crucial feature of catechins (e.g., epigallocatechin and epigallocatechin gallate) as antioxidants in diverse biological processes, also enabling the reduction of gold ions and the formation of gold nanoparticles (AuNPs).[29] The standard redox potential of $Au^0/AuCl_4^-$ ($AuCl_4^- + 3e^- = Au^0 + 4Cl^-$, $E° = 1.002$ V) is more positive than that of TA, so electrons can be donated to the Au precursors from TA while phenolic groups are oxidized to quinones.[30,31]

Polyphenols can also absorb ultraviolet (UV) light because of their π-conjugation structures.[32] The photooxidation of polyphenols has been studied under UV irradiation.[33,34] Phenol groups lose their hydrogen atoms to form quinones while hydrogen atoms are transferred to a neighboring substance, called hydrogen abstraction. This property was utilized for dye-sensitized solar cells.[35,36] When TA is photoexcited, the reversible redox reaction can occur between phenol and quinone, suggesting that TA can work as a redox coupling agent. In addition, the photooxidation of TA can cooperate with the photodecomposition of $AuCl_4^-$ ions under UV irradiation. $AuCl_4^-$ ions are excited and decomposed into $AuCl_3^-$ and a chlorine atom in water.[37] In the presence of hydrogen atom donors, the chlorine atom can be combined with a hydrogen atom to form HCl, and $AuCl_3^-$ is retained and subsequently reduced. In this situation, TA can make a hydrogen atom donor under UV irradiation.

Once AuNPs are generated through the metal reduction following metal ion adsorption on TA-coated substrates, they can also strongly absorb visible or near-infrared (NIR) light via localized surface plasmon resonance (LSPR).[38] After LSPR excitation, surface plasmons decay nonradiatively via Landau damping, producing hot carriers.[39] Hot carriers can be utilized to drive chemical reactions including catalysis and nanocrystal growth.[40−42] In particular, hot electron-driven growth of gold and silver nanocrystals have been studied to elucidate the participation of hot electrons in the reduction of metal precursors.[43−46] However, the well-known photochemical reduction of noble metal ions has never harnessed the facilitation of their selective adsorption for metal recovery.

In this work, we investigated the photochemically enhanced selective adsorption of gold ions from a mixture of metal ions, commonly found in wastewater, using TA-coated porous polymer microspheres. Porous poly(ethylene glycol dimethacrylate-*co*-acrylonitrile) (poly(EGDMA-*co*-AN) microspheres were synthesized by suspension polymerization and used as a porous substrate for TA coatings. The adsorption kinetics and isotherm for gold ions were determined to evaluate the feasibility of the TA-coated microspheres as an adsorbent. To examine the effects of light illumination, we also examined the surface chemistry and morphology of the TA-coated microspheres exposed to gold ions. The adsorption selectivity of the TA-coated microspheres was examined for 37 different metal ions, including metal ions commonly found in electronic wastewater.

2. RESULTS AND DISCUSSION

TA-Coated Porous Polymer Microspheres. Mesoporous poly(EGDMA-*co*-AN) microspheres were prepared by suspension polymerization according to our previous reports.[18,47,48] During the polymerization with toluene as a porogen, nanosized pores were created by the non-solvent-induced phase separation of the synthesized oligomers in the suspended monomer droplets. The specific area, total pore volume (V_p), and average pore diameter (D_p) of the as-synthesized poly(EGDMA-*co*-AN) microspheres (denoted as "*p*MS") were 134.6 $m^2\ g^{-1}$, 0.466 $cm^3\ g^{-1}$, and 13.8 nm, respectively, as determined by Brunauer−Emmett−Teller (BET) isotherm analysis using nitrogen gas adsorption (Figure 1A). The average pore diameter (D_p) was calculated by the equation $D_p = 4V_p/S_{BET}$, where V_p is the total pore volume and S_{BET} is the BET surface area. The results indicate that most of the pore volume of the microspheres was occupied by the mesopores <50 nm in diameter. The small pore size, high porosity, and large surface area of the produced *p*MS make them a very attractive substrate for the adsorption of metal ions.

TA can act as a polydentate ligand for metal ions to rapidly form metal-coordination complexes, so TA was introduced as an adsorption site for gold ions by deposition onto the pore surface of *p*MS. The TA coating of *p*MS was performed by a simple immersion process in an aqueous solution of TA. Briefly, the dried *p*MS was suspended in ethanol and degassed using bath-type sonication to remove air bubbles trapped in the internal pores of *p*MS. The *p*MS was collected by centrifugation and suspended in a TA solution (1 mg mL^{-1}, 100 mL). The suspension was incubated with magnetic stirring

DOI: 10.1021/acsami.9b05197
ACS Appl. Mater. Interfaces 2019, 11, 21915−21925

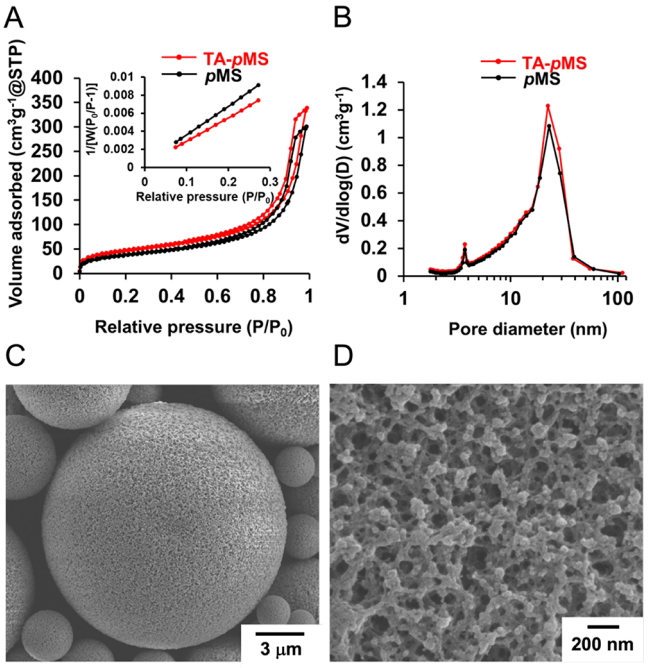

Figure 1. BET isotherms of nitrogen gas adsorption (inset: BET surface area plots) (A) and pore volume distribution (B) of *p*MS and TA-*p*MS and SEM images (C and D) of TA-*p*MS.

at room temperature for 30 min. The measured specific area and total pore volume of the TA-coated porous microspheres (denoted as "TA-*p*MS") were 164.6 $m^2\ g^{-1}$ and 0.526 $cm^3\ g^{-1}$, respectively, which were slightly larger than those of the untreated *p*MS.

In contrast, the average pore diameter of TA-*p*MS (D_p = 12.8 nm) was smaller than that of *p*MS (D_p = 13.8 nm). The results can be attributed to the formation of TA-coated layers, which can increase the roughness of the internal pores while reducing the pore size. The results also indicate that TA coatings did not block the internal pores of *p*MS. Accordingly, the pore volume distribution as a function of pore diameter was nearly the same between *p*MS and TA-*p*MS, which was obtained by the Barrett, Joyner, and Halenda (BJH) method (Figure 1B). Scanning electron microscopy (SEM) images show the highly open porous structures of TA-*p*MS as shown in Figure 1C,D.

Photoenhanced Gold Adsorption Kinetics of TA-*p*MS. Adsorption kinetics of gold ions on TA-*p*MS was investigated with 5 mg mL^{-1} of untreated *p*MS and TA-*p*MS and 10 mL of 1 mM $HAuCl_4$ at room temperature in the dark and under light illumination. Three different illumination conditions were used to explore the effects of light wavelengths on the adsorption of gold ions: AM1.5-simulated sunlight (denoted as "1-sun (full)"), 1-sun passing through a 450 nm long-pass filter (denoted as "1-sun (>450 nm)"), and 1-sun passing through a 400 nm short-pass filter (denoted as "1-sun (<400 nm)"). The adsorption profiles of gold ions were determined by monitoring the concentration of gold ions in the solution using inductively coupled plasma optical emission spectrometry (ICP-OES), and experimental data, obtained from five batches, of the number of gold ions adsorbed on *p*MS and TA-*p*MS at time t (q_t, mmol g^{-1}) depending on the adsorption time (t, min) are shown in Figure 2A. Gold ion adsorption onto TA-*p*MS was fast at the beginning and gradually slowed down regardless of the presence of light illumination. In the dark, *p*MS exhibited lower adsorption capacity than TA-*p*MS, indicating that the adsorption of gold ions by the phenolic hydroxyl groups of TA is very efficient, though the nitrile groups of *p*MS can also attract gold ions as demonstrated in our previous works.[18,48] Interestingly, 1-sun (full) light illumination significantly increased the adsorption rate of gold ions on TA-*p*MS. The result indicates that the light illumination makes the adsorption efficiency relatively faster by the photooxidation of TA, photodecomposition of $AuCl_4^-$, and hot electron transfer.

Two kinetic models were used to analyze the adsorption kinetic profiles of gold ions on *p*MS and TA-*p*MS in the dark and under light illuminations: pseudo-first-order and pseudo-second-order kinetic models. The pseudo-first-order model implies a linear driving force by one-site-occupancy adsorption while the pseudo-second-order model corresponds to two-site-occupancy adsorption at solid/solution interfaces of an adsorbent.[49,50] Mathematical equations of each kinetic model were used to examine the validity of the models using the correlation coefficient (R^2) (see Supporting Information). Values of R^2 and kinetic parameters were obtained by plotting the integral equations of each kinetic model (Figure S1A,B and Table S1). According to the small values of R^2 for *p*MS (R^2 = 0.241 and 0.561), the adsorption data of *p*MS are not in line with both kinetic models because the adsorption behavior is not clearly evident over time. In the case of TA-*p*MS, the R^2 values of the pseudo-first-order model (R^2 = 0.908−0.987) are lower than those of the pseudo-second-order model (R^2 = 0.938−0.995) regardless of the presence of light irradiation, indicating that the adsorption data were more adequately fitted to the pseudo-second-order model. It is also confirmed by fitting results of pseudo-first-order and pseudo-second-order kinetic models (Figure S1C and Figure 2A). The result suggests that gold ions interact with two adsorption sites in the galloyl group for the adsorption of gold ions on the TA layer.

The initial adsorption rates (h, mmol $g^{-1}\ min^{-1}$), calculated from the pseudo-second-order kinetic parameters, are arranged to examine the effects of irradiation on the adsorption of gold ions on TA-*p*MS as shown in Figure 2B. The value of h was increased by 2.37, 1.75, and 2.42 times under 1-sun (>450 nm) (0.018 mmol $g^{-1}\ min^{-1}$), 1-sun (<400 nm) (0.014 mmol $g^{-1}\ min^{-1}$), and 1-sun (full) (0.019 mmol $g^{-1}\ min^{-1}$), respectively, in comparison to that in the dark (0.008 mmol $g^{-1}\ min^{-1}$) for TA-*p*MS. This result indicates that both UV and visible light contributes to the elevation of the initial adsorption rate of gold ions, while the adsorption rate is more increased by visible light possibly because of the LSPR-induced hot electrons. The increase in the adsorption rate by visible light at the beginning of the adsorption suggests that AuNPs are rapidly formed by fast adsorption and reduction of gold ions and interact with visible light. The highest value of h under 1-sun (full) is ascribed to the cooperation between UV and visible light.

Photoenhanced Gold Adsorption Isotherm of TA-*p*MS. The adsorption isotherms of gold ions were investigated using 5 mg mL^{-1} of untreated *p*MS and TA-*p*MS and 3 mL of 0.25, 0.33, 0.5, 1, 1.5, and 2 mM $HAuCl_4$ for 3 h at room temperature in the dark and under light illumination. The adsorption profiles of gold ions were determined by monitoring the concentration of gold ions in the solution using ICP-OES. The number of gold ions adsorbed on *p*MS and TA-*p*MS (q, mmol g^{-1}) is represented as a function of the concentration (C, mM) of gold ion (Figure 2C). The number of gold ions adsorbed on TA-*p*MS was larger than that on

DOI: 10.1021/acsami.9b05197
ACS Appl. Mater. Interfaces 2019, 11, 21915−21925

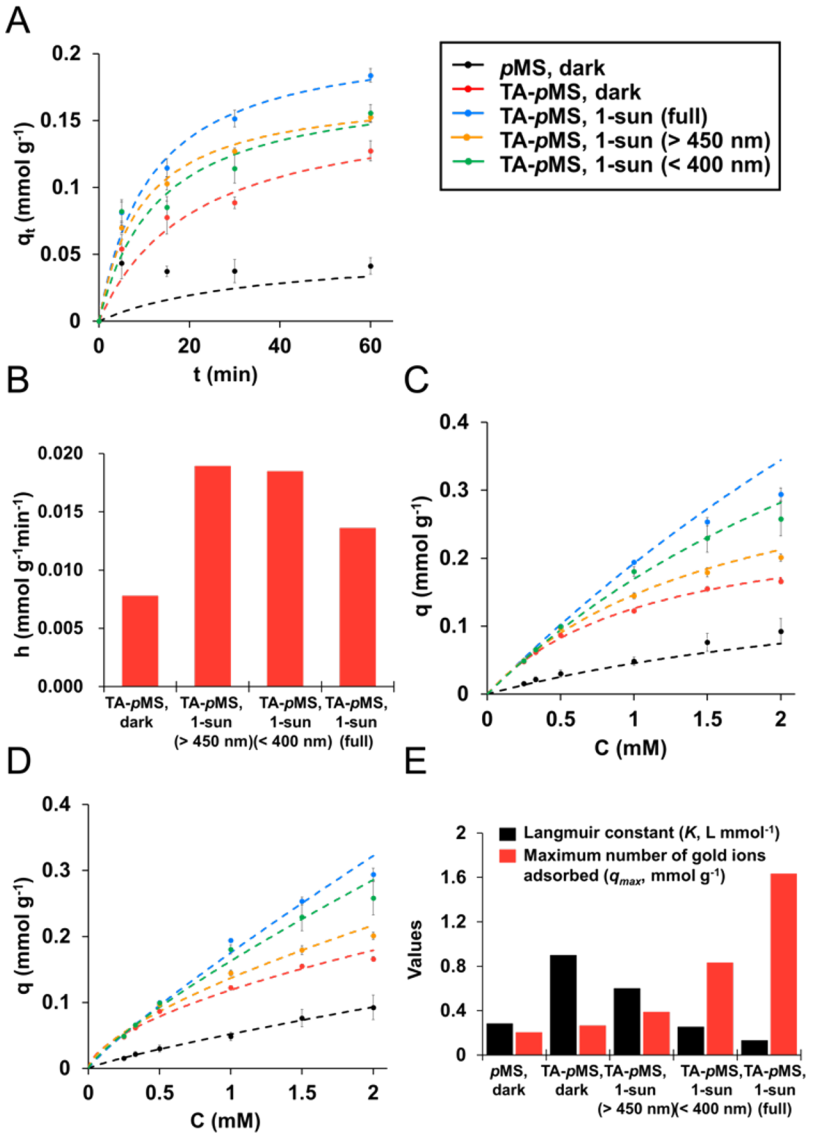

Figure 2. (A) Adsorption kinetics of gold ions on *p*MS and TA-*p*MS (points, experimental data; dashed lines, results of the pseudo-second-order model fitting). (B) Initial adsorption rates of gold ions on TA-*p*MS calculated from the pseudo-second-order model. (C) Adsorption isotherm of gold ions on *p*MS and TA-*p*MS (points, experimental data; dashed lines, results of Langmuir isotherm fitting). (D) Adsorption isotherm of gold ions on *p*MS and TA-*p*MS (points, experimental data; dashed lines, results of Freundlich isotherm fitting). Box: legends for (A, C, and D). (E) Langmuir isotherm parameters of adsorption of gold ions on and *p*MS and TA-*p*MS in the dark and under illumination.

*p*MS, indicating that the surface modification with TA improved adsorption capacity. Interestingly, the number of gold ions adsorbed substantially increased under irradiation. The experimental data were fitted to the Langmuir and Freundlich isotherm models to examine the adsorption behaviors of gold ions in more detail. The Langmuir isotherm model describes adsorption at equivalent sites that have the same affinity for adsorbates that leads to the formation of a monolayer.[51] The Freundlich isotherm model describes adsorption at heterogeneous surfaces that have the nonequal affinity for adsorbates to form a multilayer.[51] Linearized equations of each isotherm model were used to investigate the validity of the models (see Supporting Information). Isotherm parameters calculated from each isotherm model are summarized in Table S3. According to the correlation coefficients (R^2), experimental adsorption data were better fitted to the Langmuir isotherm (R^2 > 0.99) than the Freundlich isotherm (R^2 = 0.980−0.995) for *p*MS and TA-*p*MS regardless of the presence of light irradiation.

Figure 2C,D shows the fitting results of Langmuir and Freundlich isotherms under different illumination conditions. Interestingly, Langmuir fitting curves overestimate the experimental data compared to Freundlich fitting curves at the high concentrations (1.5 and 2 mM) under light irradiation. The fitting results indicate that the Freundlich isotherm model is more appropriate, at least for the high-concentration regime under light irradiation. As a result, the Langmuir isotherm properly evaluates the adsorption of gold ions on TA-*p*MS in the low-concentration regime in which the formation of a monolayer is feasible via the adsorption of gold ions at homogeneous sites. In the high-concentration regime, the Freundlich isotherm indicates that heterogeneous adsorption sites spread on TA-*p*MS to form a multilayer as the nucleation of fully reduced gold ions and the formation of AuNPs take places.

DOI: 10.1021/acsami.9b05197
ACS Appl. Mater. Interfaces 2019, 11, 21915−21925

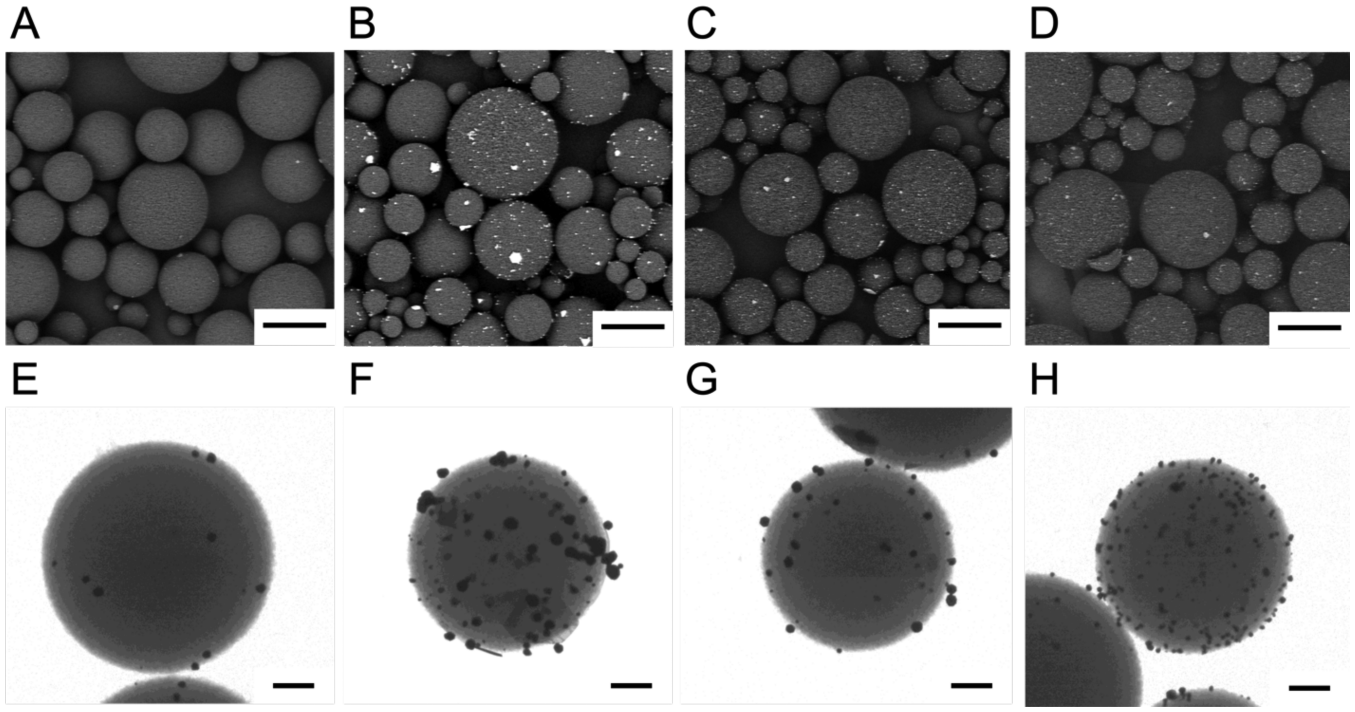

Figure 3. SEM (A–D) and TEM (E–H) images of Au-TA-*p*MS obtained from gold adsorption experiments for 3 h in 1 mM $HAuCl_4$ solution in the dark (A and E) and under 1-sun (full) (B and F), 1-sun (>450 nm) (C and G), and 1-sun (<400 nm) illuminations (D and H). Scale bars: 10 μm (A–D) and 1 μm (E–H).

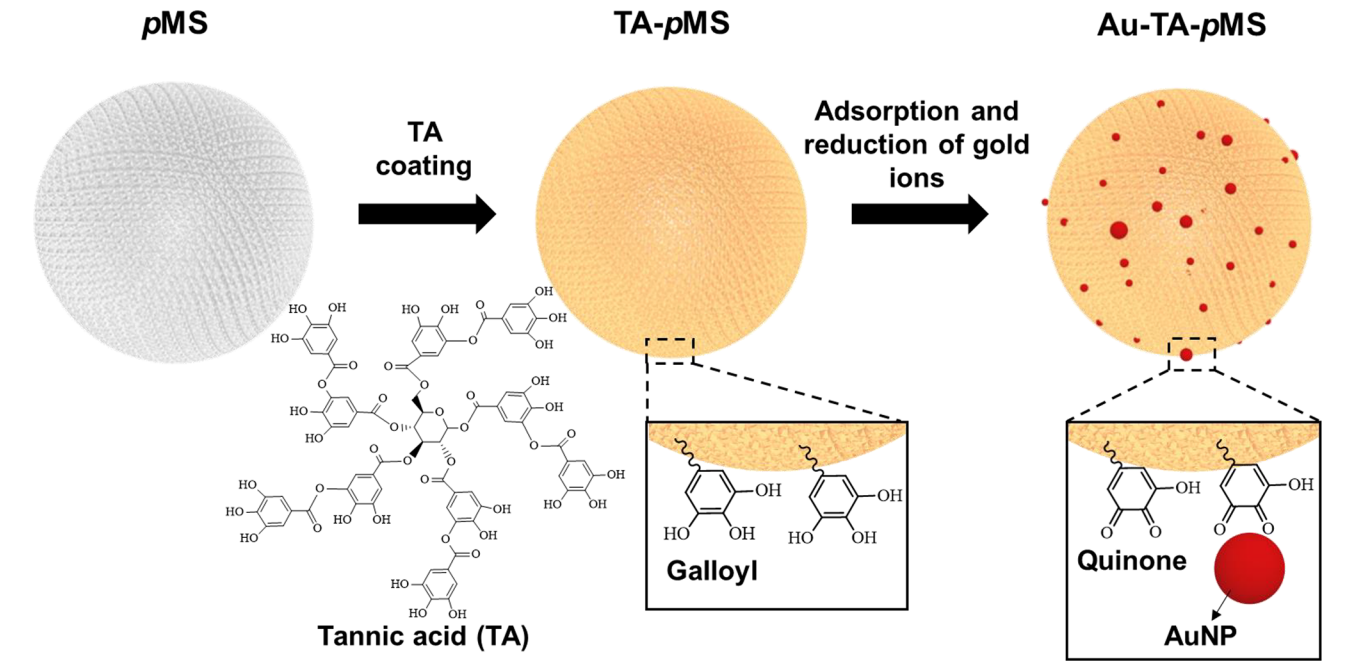

Figure 4. Schematic illustration of the adsorption and reduction of gold ions on TA-*p*MS.

On the other hand, the theoretical maximum number (q_{max}, mmol g^{-1}) of gold ions adsorbed per unit mass of *p*MS and TA-*p*MS and Langmuir constants (K, L $mmol^{-1}$) are arranged in Figure 2E. The increased value of q_{max} for TA-*p*MS (0.266 mmol g^{-1}) shows that TA coating on *p*MS enhances the adsorption capacity compared to that for *p*MS (0.204 mmol g^{-1}). The value of q_{max} was increased by 1.46, 3.12, and 6.13 times under 1-sun (>450 nm) (0.389 mmol g^{-1}), 1-sun (<400 nm) (0.833 mmol g^{-1}), and 1-sun (full) (1.635 mmol g^{-1}), respectively, in comparison to that in the dark (0.266 mmol g^{-1}) for TA-*p*MS. The results indicate that UV light greatly contributed to the increased gold adsorption capacity, though the adsorption capacity was also increased by visible light. Under 1-sun (full), q_{max} was remarkably increased, presumably through a synergistic effect of UV and visible light illumination. The Langmuir constant (K) of TA-*p*MS was larger than that of *p*MS, indicating that TA layers increase the binding affinity for gold ions compared to the nitrile groups of *p*MS. In addition, it

DOI: 10.1021/acsami.9b05197
ACS Appl. Mater. Interfaces 2019, 11, 21915–21925

is reasonable that K decreased with irradiation, unlike q_{max}, which is attributed to the decreased binding affinity for gold ions with the adsorption sites being more filled by the increased number of gold ions adsorbed. Consequently, it was confirmed that the adsorption capacity of TA-*p*MS was significantly enhanced under irradiation.

Photochemical Adsorption and Reduction of Gold Ions. Scanning electron microscopy (SEM) images by backscattered electrons (BSE) detection were used to examine the formation of AuNPs on TA-*p*MS. SEM images (Figure 3A−D) indicate that a much larger number of AuNPs were generated under light illumination. Higher magnification SEM images (Figure S3) show that a mixture of spherical, triangular, and hexagonal AuNPs with a highly polydisperse size distribution was generated. The broad size distribution is probably attributed to irregular and random coalescence, indicating that TA deposited onto the surfaces of *p*MS did not act as a stabilizing agent. Representative transmission electron microscopy (TEM) images are also shown in Figure 3E−H, which clearly show the size polydispersity of AuNPs on Au-adsorbed TA-*p*MS (denoted as "Au-TA-*p*MS"). The large values of all of the relative standard deviations (>20%) indicate the high polydispersity of the particle size except Au-TA-*p*MS under 1-sun (<400 nm) illumination (Figure S4). In the dark, AuNPs were sparsely populated on TA-*p*MS with a diameter ranging from 53 to 253 nm (the average diameter = 156.2 ± 61.0 nm). By contrast, AuNPs were densely populated with a larger size polydispersity ranging from 90 nm to 1.2 μm (280.9 ± 197.6 nm) under 1-sun (full) illumination. Under 1-sun (>450 nm) illumination, medium-sized AuNPs, ranging from 90 to 320 nm (183.36 ± 59.8 nm), were closely populated, while a larger number of smaller AuNPs, ranging from 75 to 150 nm (111.7 ± 21.1 nm), were densely populated under 1-sun (<400 nm) illumination.

The existence of AuNPs on TA-*p*MS regardless of the presence of light irradiation confirmed that gold ions were adsorbed and reduced by galloyl or catechol groups of TA on TA-*p*MS while phenolic hydroxyl groups were oxidized to quinones as illustrated in Figure 4. The oxidation of phenolic hydroxyl groups to quinones was investigated using Fourier-transform infrared spectroscopy (FT-IR) analysis for TA and AuNPs which were synthesized by adding gold ion precursors in a TA solution (denoted as "TA-AuNPs") (Figure S5). FT-IR spectra exhibit the formation of quinone for TA-AuNPs during the reduction of gold ions because of a peak shift from 1710 cm^{-1} (C═O ester stretching) to 1703 cm^{-1} (aromatic C═O stretching) and a new peak at 1136 cm^{-1} (C═O stretching), as reported in previous studies.[52,53] The reduction of gold ions can be followed by several events simultaneously: the nucleation of metallic gold atoms, the growth of gold nuclei, and the coalescence of neighboring gold nuclei. Accordingly, UV and visible light can induce different effects on the adsorption behavior of gold ions, and the generated AuNPs may have different size and spatial distributions. UV light increases the adsorption and reduction rate of gold ions by TA, which may lead to the nucleation of gold atoms. TA-mediated nucleation seems to take place at a large number of sites simultaneously as many smaller AuNPs were observed under 1-sun (<400 nm) illumination in comparison to those in the dark and 1-sun (>450 nm) illumination. This phenomenon can be explained by the photooxidation of TA and photodecomposition of $AuCl_4^-$ ions under UV irradiation, which can facilitate the reduction of gold ions. Visible light illumination increased the growth rate of AuNPs by hot electrons generated on the surface of AuNPs as described in a previous report.[43] As a result, larger AuNPs were observed under 1-sun (>450 nm) illumination compared to that in the dark and 1-sun (<400 nm) illumination. The work function of gold is near 5.5 eV, converted to the position of Fermi level of 1 V vs NHE, which is located around the same level with the reduction potential of Au precursors.[54] Thus, under light illumination, electron transfer from AuNPs to Au precursors is a thermodynamically downhill reaction considering their redox potentials, and hot electron transfer is favorable. Under 1-sun (full) illumination, the combined effects of UV and visible lights accelerated both nucleation and growth of AuNPs, efficiently increasing the adsorption capacity of TA-*p*MS.

Light absorption spectra were obtained using an integrating sphere to correct reflection for *p*MS, TA-*p*MS, and Au-TA-*p*MS (Figure 5). TA-*p*MS show strong UV absorption with a peak of 216 nm due to electronic transitions in the π-conjugated system of TA compared to the untreated *p*MS. Au-TA-*p*MS exhibited the increased absorption in visible- and NIR-light ranges due to LSPR by AuNPs formed on the TA layer. The generated AuNPs exhibited a broad absorption peak around 525 nm, indicating that the average diameter of colloidal AuNPs was about 20 nm, though the size distribution was very wide. The absorption peak of TA was slightly blue-shifted in the Au-TA-*p*MS probably because of the change of refractive index around TA by the formation of AuNPs. The optical changes of Au-TA-*p*MS indicate that the gold ion adsorption was photochemically enhanced through the generation of hot electrons in the TA layer.

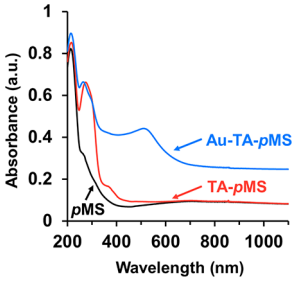

Figure 5. Light absorption spectra of *p*MS, TA-*p*MS, and Au-TA-*p*MS measured using the integrating sphere.

Effects of Light Irradiation on the Oxidation States of Gold Species Adsorbed on TA-Coated Microspheres. X-ray photoelectron spectroscopy (XPS) was used to examine the surface chemistry of TA-*p*MS after gold ion adsorption experiments and the changes in the oxidation states of the adsorbed gold (Figure 6A). Gold adsorption experiments were conducted using 1 mM $HAuCl_4$ for 3 h under light illumination or in the dark. Au 4f level was split into Au $4f_{5/2}$ and $4f_{7/2}$ by 3.7 eV because of spin−orbit splitting. Au 4f peaks of Au^0 were observed at 84.0 and 87.7 eV, indicating the reduction of gold ions by TA. The peaks for Au^{1+} and Au^{3+} are ascribed to the complexation of gold ions with the galloyl (*o*-triphenol) group of TA. The atomic percentages of gold species were calculated by integrating the peak areas of Au^0, Au^+, and Au^{3+}, respectively (Figure 6B). The atomic percentage of metallic gold (Au^0) was much higher when the adsorption experiments were performed under light illumination. TA is a polyphenolic compound containing gallic acid esters, which has a standard reduction potential of 0.897 V vs

DOI: 10.1021/acsami.9b05197
ACS Appl. Mater. Interfaces 2019, 11, 21915−21925

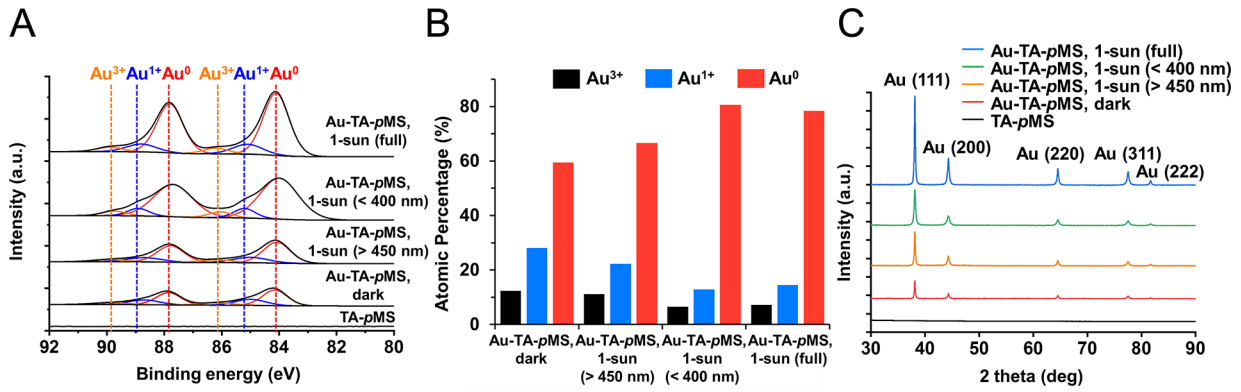

Figure 6. (A) XP spectra for Au-TA-*p*MS in the dark and under light illumination. (B) Atomic percentages of Au species depending on irradiation conditions obtained through the area of the Au species peak from the XP spectra. (C) XRD plots for Au-TA-*p*MS in the dark and under illumination.

NHE.[29] TA can be oxidized through two successive proton-coupled electron transfers (PCET) that can lead to the reduction of metal ion complexes. It was hypothesized that the reduction process is facilitated by the UV light absorption of TA, which can provide high-energy electrons to gold ion complexes, resulting in the increased reduction of the adsorbed Au ion species into metallic Au nanostructures. The reduction of gold ions to metallic gold was also confirmed by X-ray diffraction (XRD) analysis of Au-TA-*p*MS (Figure 6C). XRD patterns of Au-TA-*p*MS exhibited five peaks at 2θ = 38.14°, 44.33°, 64.54°, 77.53°, and 81.68°, which correspond to (111), (200), (220), (311), and (222) planes of the face-centered cubic lattice of gold, respectively. The results suggest that a redox reaction between TA-*p*MS and gold ions causes the reduction of gold ions to metallic gold.

Mechanism of Photochemical Adsorption and Reduction of Gold Ions. We propose a mechanism for the photochemical adsorption and reduction of gold ions under irradiation as summarized in Figure 7. In the dark, the galloyl group is oxidized to form quinone by PCET, while gold ions are reduced by accepting the electrons because of the difference of the redox potentials between gold ions and TA as illustrated in Figure 7A.[55−57] Neighboring galloyl groups participate in the reduction reaction of gold ions, which is required to cause three electron transfers from TA to $AuCl_4^-$ (Au^{3+}) to form metallic gold (Au^0), as described in the reaction (2). Under 1-sun (>450 nm) illumination, gold ions are reduced in the same manner at the beginning of the adsorption, but the reduction of gold ions is accelerated by hot electron transfer from AuNPs to gold ions to cause the growth of AuNPs because of the difference between electronic energies of AuNPs and gold ions. Under 1-sun (<400 nm) illumination, the reduction of gold ions takes place in a completely different manner at the beginning of adsorption because of the photooxidation of TA and photolysis of $AuCl_4^-$ ions (Figure 7B). Upon the absorption of UV light via ligand-to-metal charge transfer, $AuCl_4^-$ ion is excited and decomposed to $AuCl_3^-$ and a chlorine atom, as described in the reaction (3), while the decomposed state is so reactive and unstable that $AuCl_3^-$ and the chlorine atom can recombine.[37,58] A hydrogen atom is provided to the chlorine atom by TA via the photooxidation of TA to produce HCl, while TA has a semiquinone radical through the reaction (4). Subsequently, $AuCl_3^-$ is reduced to $AuCl_2^-$ by another phenol group via the photooxidation of TA to result in the formation

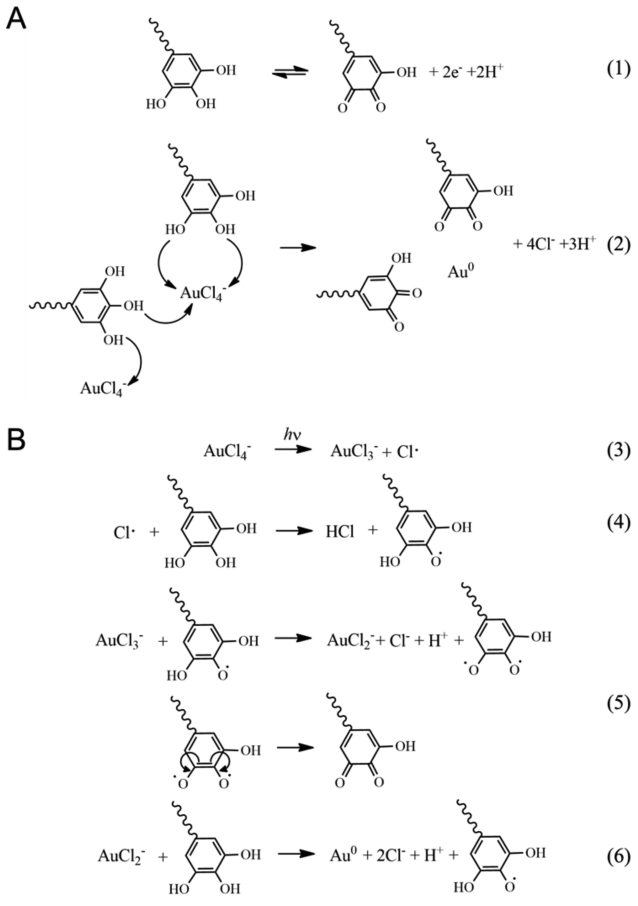

Figure 7. Schematic illustration of the mechanism of adsorption and reduction of gold ions by TA in the dark and under 1-sun (>450 nm) illumination (A) and under 1-sun (full) and 1-sun (<400 nm) illumination (B).

of a quinone through the reaction (5), followed by the reduction of $AuCl_2^-$ to metallic gold via the photooxidation of TA as shown in the reaction (6). Therefore, the initiation of the reduction of gold ions and the successive reduction processes of gold ions are promoted by the photolysis of $AuCl_4^-$ ions and photooxidation of TA, respectively.

Metal Adsorption Selectivity and Stability of TA-*p*MS. Electronic waste, typically printed circuit boards, and industrial waste from catalysts and jewelry contain a variety of precious

DOI: 10.1021/acsami.9b05197
ACS Appl. Mater. Interfaces 2019, 11, 21915−21925

metals (e.g., Au, Ag, Pt, and Pd) and base metals (e.g., Fe, Ni, Cu, Zn, and Sn), so selective metal adsorption for metals with higher priority is required.[59−61] From this perspective, we investigated the metal adsorption selectivity of TA-*p*MS using two multielement ICP standard solutions: standard solution 1 (Sb, Au, Hf, Ir, Pd, Pt, Rh, Ru, Te, and Sn in 10% HCl and 1% HNO_3) and standard solution 2 (Li, Be, Na, Mg, Al, K, Ca, V, Cr, Mn, Fe, Co, Ni, Cu, Zn, Ga, As, Se, Rb, Sr, Ag, Cd, Cs, Ba, Tl, Pb, and U in 5% HNO_3). TA-*p*MS (2 mg mL^{-1}) was dispersed in 10 mL of each of the standard solutions containing 100 ppb metal species. TA-*p*MS was immersed in the standard solutions for 3 and 24 h in the dark and under 1-sun (full) illumination. The adsorption efficiency of the metal species on TA-*p*MS was determined by monitoring the gold ion concentration using inductively coupled plasma mass spectrometry (ICP-MS).

The adsorption efficiencies for ten metal ions most commonly found in electronic and industrial waste are summarized in Figure 8, arranged from Figure S5A,B. TA-

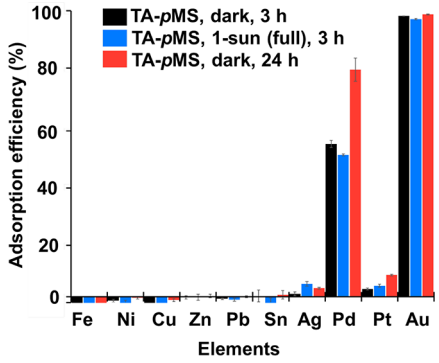

Figure 8. Adsorption percentages of various metals on TA-*p*MS at different incubation times and under different irradiation conditions.

*p*MS exhibited a high adsorption efficiency (98%) and notable selectivity toward gold for 3 h in the dark. No other metal ions exhibited adsorption except Pd (53%). In the media of solution 1 containing HCl and HNO_3, Au and Pt generally form chloro-complexes such as $AuCl_4^-$ and $PtCl_4^{2-}$ or $PtCl_6^{2-}$ with Cl ligands, respectively, which is less dependent on concentrations of Cl^-.[62] However, Pd forms different species such as Pd^{2+}, $PdCl^+$, $PdCl_3^-$, and $PdCl_4^{2-}$ depending on the concentrations of Cl^-.[62,63] Ag exists as a cation, which is Ag^+, without a ligand in the media of the solution 2 containing HNO_3. $AuCl_4^-$ has a relatively higher standard redox potential ($E°$ = 1.002 V for $Au^0/AuCl_4^-$) than other precious metal species ($E°$ = 0.799 V for Ag^0/Ag^+; $E°$ = 0.76 V for $Pt^0/PtCl_4^{2-}$; $E°$ = 0.68 V for $PtCl_4^{2-}/PtCl_6^{2-}$; $E°$ = 0.92 V for Pd^0/Pd^{2+}; and $E°$ = 0.62 V for $Pd^0/PdCl_4^{2-}$) and base metals with $E°$ < 0.6 V.[28,64,65] The higher redox potential facilitates the reduction of gold ions by TA, which can be a driving force for the selective adsorption of Au. In the case of Pd, it is presumed that Pd^{2+} is adsorbed on TA-*p*MS, as reported in previous studies demonstrating reduction of Pd^{2+} to Pd^0 to form Pd nanoparticles using TA and gallic acid as a reducing agent.[66,67] In addition, it is known that the galloyl group chelates base metal ions (e.g., Fe, Cu, and Zn) to form complexes; however, its reversibility restricts the efficient adsorption of base metal ions by TA.[55,68] For some metal ions, negative values of the adsorption efficiency were obtained, which is presumably because of the contamination of experimental tools by trace metal ions. Despite 1-sun (full) illumination, only Au ions significantly exhibited a high level of adsorption, while Pd ions showed moderate adsorption efficiency which is nearly the same as that in the dark. The results indicate that TA has high selectivity toward gold ions, particularly under light illumination, among other metal ions, although various metal ions can bind to TA if no competitive condition is given. In addition, the influence of light on the metal precursor, like the gold precursor ion, can play an important role in the metal adsorption. The adsorption efficiency of Pd was increased when the solution was incubated for a longer time, indicating that the adsorption kinetics of Pd ions by TA is much slower than that of Au ions because of the more favorable reduction potential of Au. On the other hand, the mixture of the standard solutions was also used to examine the adsorption competition among all the metal ions, and the results of the adsorption efficiencies showed little difference in metal selectivity but for Ag (Figure S6C,D). The difference in the adsorption efficiency for Ag is possibly due to the formation of AgCl produced by mixing two standard solutions, of which one contains HCl. As a result, it can be said that TA-*p*MS is a gold adsorbent with excellent selectivity and fast kinetics, which harnesses photochemical pathways for higher adsorption capacity.

Stability of TA-*p*MS was also investigated to confirm the applicability as an adsorbent depending on incubation time. TA-*p*MS was dispersed in deionized water for the different incubation times, which is 0.1, 24, and 48 h, and used for adsorption experiments of gold ions to explore whether the TA layer is detached from TA-*p*MS and the adsorption efficiency is affected. As shown in Figure S7, the adsorption efficiency slightly decreased but remained at ∼94% compared to that of the freshly prepared TA-*p*MS, as obtained from ICP-OES. Therefore, the TA layer is very stable, and the adsorption efficiency was well maintained. In addition, the stability of TA-*p*MS during desorption of gold was investigated by conducting adsorption and desorption experiments using 1 mM $HAuCl_4$ under 1-sun (full) and Au leaching by thiourea, respectively. SEM images by BSE detection confirmed that gold was desorbed from TA-*p*MS by thiourea as shown in Figure S8, and desorption efficiency was 99.4 ± 0.07%, as measured by ICP-OES. After the desorption experiments, the second adsorption experiments were conducted, and adsorption capacity was 199.1 ± 0.4 and 199.6 ± 0.1 μmol g^{-1} for the first and second adsorption experiments, respectively, as determined from ICP-OES. Therefore, the adsorption capacity was nearly the same, ensuring the stability during the desorption of gold and further recycled use of TA-*p*MS.

3. CONCLUSIONS

This work demonstrated that tannin-coated porous microspheres could serve as an excellent adsorbent for gold ion recovery through photochemical reduction. It has been known that tannin has a high affinity for various metal ions and a mild redox potential that can reduce some metal ions. However, this work revealed, for the first time, that the light absorption, particularly in the UV range, can activate tannin to reduce gold ions into metallic gold selectively. The 1-sun simulated light illumination increased the maximum number of adsorbed gold ions by 6.1 times. We expect that tannin-coated porous substrates are a promising candidate for practical applications to the efficient and selective recovery of gold ions from electronic and other industrial wastewater.

DOI: 10.1021/acsami.9b05197
ACS Appl. Mater. Interfaces 2019, 11, 21915−21925

4. EXPERIMENTAL METHODS

Materials. Ethylene glycol dimethacrylate (EGDMA), acrylonitrile (AN), tannic acid (TA), gold(III) chloride trihydrate ($HAuCl_4 \cdot 3H_2O$), thiourea ($CS(NH_2)_2$), and sulfuric acid (H_2SO_4) were purchased from Sigma-Aldrich (St. Louis, USA). Poly(vinyl alcohol) (PVA, $M_w = 8.8–9.2 \times 10^4$ g mol^{-1}, 87–89% degree of saponification) was purchased from Kuraray Co. (Kurashiki, Okayama, Japan). 2,2′-Azobis(2,4-dimethyl valeronitrile) (ADVN, Wako Pure Chemicals Industries, Ltd., Osaka, Japan) was recrystallized from methanol before use. Ethanol (94.5%) was purchased from Daejung Chemicals (Siheung, Republic of Korea). Multielement standard solutions for ICP-MS were purchased from Agilent (Santa Clara, CA, USA). Milli-Q water was used as deionized water in all experiments. Isopropanol was obtained from Samchun Pure Chemical Co., Ltd. (Pyeongtaek-si, Republic of Korea).

Preparation of Poly(EGDMA-*co*-AN) Porous Microspheres. Mesoporous poly(EGDMA-*co*-AN) microspheres were prepared by suspension polymerization synthesis as previously reported.[18,47,48] First, a mixture of EGDMA (50 wt %), AN (10 wt %), and ADVN (1 wt % against total monomer), and toluene was emulsified in a 1 wt % PVA solution using a homogenizer. To induce the formation of internal pores within *p*MS, we added 40 wt % toluene to the solution. The prepared mixture was transferred to a double-walled glass reactor equipped with a stirrer, a reflux condenser, thermocouples, and a nitrogen gas inlet system. The polymerization in the aqueous phase was suppressed using a small amount of sodium nitrite (0.01 wt %). The polymerization was carried out at 60 °C for 10 h at 250 rpm. The synthesized *p*MS was collected by filtration, repeatedly washed using methanol, and dried in a vacuum.

Preparation of TA-Coated Porous Microspheres. The prepared *p*MS (1 g) was dispersed in 100 mL of ethanol using bath-type sonication for 10 min and magnetic stirring at 300 rpm for 50 min at room temperature to increase the wettability of *p*MS. Ethanol was removed by swing-type centrifugation at 1000*g* for 3 min, and then *p*MS was washed using immersion in deionized water. The *p*MS was immersed in 100 mL of a TA solution (10 mg mL^{-1}) with magnetic stirring at 1000 rpm for 30 min at room temperature. TA-*p*MS was collected by swing-type centrifugation at 1000*g* for 3 min. TA-*p*MS was repeatedly washed with a 7:3 (v/v) mixture of ethanol and deionized water using repetitive centrifugation at 1000*g* for 3 min to remove excess TA unbound to *p*MS. TA-*p*MS was dried in a vacuum.

Photoenhanced Gold Adsorption Kinetics. The prepared *p*MS and TA-*p*MS were immersed in deionized water at a concentration of 10 mg mL^{-1}. An aqueous solution of 10 mM $HAuCl_4$ was prepared. Mixtures of the $HAuCl_4$ solution and the dispersion of *p*MS and TA-*p*MS were produced at a concentration of 1 mM $HAuCl_4$ and 5 mg mL^{-1} of the dispersion of *p*MS and TA-*p*MS to make 10 mL of total volume. The mixtures were magnetically stirred at 300 rpm at room temperature in the dark and under illumination conditions: 1-sun (full), 1-sun (>450 nm), and 1-sun (<400 nm). AM 1.5-simulated sunlight was applied to the mixtures using a solar simulator (Asahi Spectra HAL-320). At adsorption times of 5, 15, 30, and 60 min, 1 mL of the mixture was extracted. The *p*MS and TA-*p*MS were collected by centrifugation at 1000*g* for 3 min, and the supernatants were filtered using Minisart syringe filters with a pore diameter of 0.45 μm. The filtered supernatants were diluted with 10 M HCl to analyze the concentration of gold ions using ICP-OES (Agilent ICP-OES 5110). The collected *p*MS and TA-*p*MS were dried in a vacuum. The dried *p*MS and TA-*p*MS were repeatedly washed with deionized water by centrifugation at 1000*g* for 3 min and used for various characterizations.

Photoenhanced Gold Adsorption Isotherm. The prepared *p*MS and TA-*p*MS were immersed in deionized water at a concentration of 10 mg mL^{-1}. An aqueous solution of 10 mM $HAuCl_4$ was prepared. Mixtures of the $HAuCl_4$ solution and the dispersion of *p*MS and TA-*p*MS were produced at a concentration of 0.25, 0.33, 0.5, 1, 1.5, and 2 mM $HAuCl_4$ and 5 mg mL^{-1} of the dispersion of *p*MS and TA-*p*MS to make 3 mL of total volume. The mixtures were stirred every hour at room temperature in the dark and under 1-sun (full), 1-sun (>450 nm), and 1-sun (<400 nm). The *p*MS and TA-*p*MS were collected by centrifugation at 1000*g* for 3 min, and the supernatants were filtered using the syringe filters with a pore diameter of 0.45 μm. The filtered supernatants were diluted with 10 M HCl to analyze concentrations of remaining gold ions using ICP-OES. The collected *p*MS and TA-*p*MS were dried in a vacuum. The dried *p*MS and TA-*p*MS were repeatedly washed with deionized water by centrifugation at 1000*g* for 3 min and used for various characterizations.

Metal Selectivity of TA-Coated Microspheres. Multielement ICP standard solutions were used to investigate metal selectivity of TA-*p*MS at a concentration of 0.01 mg L^{-1}. Two standard solutions were used: standard solution 1 (Sb, Au, Hf, Ir, Pd, Pt, Rh, Ru, Te, and Sn in 10% HCl and 1% HNO_3) and standard solution 2 (Li, Be, Na, Mg, Al, K, Ca, V, Cr, Mn, Fe, Co, Ni, Cu, Zn, Ga, As, Se, Rb, Sr, Ag, Cd, Cs, Ba, Tl, Pb, and U in 5% HNO_3). TA-*p*MS was immersed in 10 mL of each standard solution and a mixture of the standard solutions at a concentration of 2 mg mL^{-1} and then mixed with magnetic stirring at 300 rpm at room temperature. TA-*p*MS was collected by centrifugation at 1000*g* for 3 min, and the supernatants were filtered using the syringe filters with a pore diameter of 0.45 μm. The filtered supernatants were analyzed to measure the remaining metal ions using ICP-MS.

Stability of TA-Coated Microspheres. TA-*p*MS was immersed in deionized water for different incubation times, 0.1, 24, and 48 h, at a concentration of 10 mg mL^{-1}. After the incubation, adsorption experiments were conducted in the same manner described above with 1 mM $HAuCl_4$ and the dispersion of 5 mg mL^{-1} of TA-*p*MS. Desorption experiments of gold were carried out using thiourea as a leaching agent and dispersion of Au-TA-*p*MS was prepared with 1 mM $HAuCl_4$ under 1-sun (full). Thiourea solution was prepared by dissolving thiourea in an aqueous solution of 0.2 M sulfuric acid at the concentration of 1 M. Au-TA-*p*MS was immersed in deionized water at a concentration of 2 mg mL^{-1}. Mixtures of the thiourea solution and the dispersion of Au-TA-*p*MS were produced at a concentration of 0.5 M thiourea and 1 mg mL^{-1} of the dispersion of Au-TA-*p*MS. The mixtures were magnetically stirred at 300 rpm at room temperature in the dark. Au-TA-*p*MS was collected by centrifugation at 1000*g* for 3 min, and the supernatants were filtered using the syringe filters with a pore diameter of 0.45 μm. The filtered supernatants were used to analyze concentrations of the remaining gold ions using ICP-OES. The collected Au-TA-*p*MS was dried in a vacuum.

Characterizations. A surface area and pore size analyzer (Micromeritics 3Flex) was used to investigate surface areas and pore sizes of *p*MS and TA-*p*MS. A UV–vis–NIR spectrometer (PerkinElmer Lambda 1050) was used for measuring the absorbance of *p*MS and TA-*p*MS with an integrating sphere. A field emission TEM (FEI Company Tecnai F20) was used with an accelerating voltage of 300 kV for analyzing the size and shape of AuNPs on TA-*p*MS. SEM images were obtained by field emission SEM (Hitachi SU5000) with an accelerating voltage of 5 kV for TA-*p*MS and Au-TA-*p*MS. FT-IR (Jasco FT/IR-6100) was used to analyze chemical structures of TA before and after the reduction of gold ions. XPS (Thermo VG scientific Sigma Probe) was used to analyze oxidation states of gold on Au-TA-*p*MS with 4 kV and 5 μA. High-resolution powder XRD (Rigaku SmartLab) was used to detect metallic gold on Au-TA-*p*MS with 45 kV and 200 mA using $\theta/2\theta$ scan.

■ ASSOCIATED CONTENT

Supporting Information

The Supporting Information is available free of charge on the ACS Publications website at DOI: 10.1021/acsami.9b05197.

Description of adsorption kinetics and isotherm of gold ions on TA-*p*MS; additional SEM images, particle size distribution histogram, and adsorption percentages of various metals on TA-*p*MS (PDF)

DOI: 10.1021/acsami.9b05197
ACS Appl. Mater. Interfaces 2019, 11, 21915–21925

AUTHOR INFORMATION

Corresponding Authors

*E-mail: yoonsung@kaist.ac.kr (Y.S.N.).
*E-mail: kjwoong@hanyang.ac.kr (J.W.K.).

ORCID

Jeonga Kim: 0000-0001-6252-0835
Kyeong Rak Kim: 0000-0001-8007-6272
Yeongran Hong: 0000-0003-3288-3066
Cafer T. Yavuz: 0000-0003-0580-3331
Jin Woong Kim: 0000-0002-2823-8825
Yoon Sung Nam: 0000-0002-7302-6928

Notes

The authors declare no competing financial interest.

ACKNOWLEDGMENTS

This work was financially supported by CTK Cosmetics (Republic of Korea) and Basic Science Research Program and Nano·Material Technology Development Program through the National Research Foundation of Korea (NRF) funded by the Ministry of Science, ICT & Future Planning (NRF-2017M3A7B4042235).

REFERENCES

(1) Kaya, M. Recovery of Metals and Nonmetals from Electronic Waste by Physical and Chemical Recycling Processes. *Waste Manage.* **2016**, *57*, 64−90.
(2) Cui, J.; Zhang, L. Metallurgical Recovery of Metals from Electronic Waste: A Review. *J. Hazard. Mater.* **2008**, *158* (2−3), 228−256.
(3) Won, S. W.; Kotte, P.; Wei, W.; Lim, A.; Yun, Y. S. Biosorbents for Recovery of Precious Metals. *Bioresour. Technol.* **2014**, *160*, 203−212.
(4) Syed, S. Recovery of Gold from Secondary Sources-A Review. *Hydrometallurgy* **2012**, *115*−*116*, 30−51.
(5) Mack, C.; Wilhelmi, B.; Duncan, J. R.; Burgess, J. E. Biosorption of Precious Metals. *Biotechnol. Adv.* **2007**, *25* (3), 264−271.
(6) Dong, Z.; Liu, J.; Yuan, W.; Yi, Y.; Zhao, L. Recovery of Au(III) by Radiation Synthesized Aminomethyl Pyridine Functionalized Adsorbents Based on Cellulose. *Chem. Eng. J.* **2016**, *283*, 504−513.
(7) Lam, K. F.; Yeung, K. L.; McKay, G. An Investigation of Gold Adsorption from a Binary Mixture with Selective Mesoporous Silica Adsorbents. *J. Phys. Chem. B* **2006**, *110* (5), 2187−2194.
(8) Lam, K. F.; Fong, C. M.; Yeung, K. L.; Mckay, G. Selective Adsorption of Gold from Complex Mixtures Using Mesoporous Adsorbents. *Chem. Eng. J.* **2008**, *145* (2), 185−195.
(9) Dogan, N. A.; Hong, Y.; Ozdemir, E.; Yavuz, C. T. Nanoporous Polymer Microspheres with Nitrile and Amidoxime Functionalities for Gas Capture and Precious Metal Recovery from E-Waste. *ACS Sustainable Chem. Eng.* **2019**, *7* (1), 123−128.
(10) You, I.; Kang, S. M.; Lee, S.; Cho, Y. O.; Kim, J. B.; Lee, S. B.; Nam, Y. S.; Lee, H. Polydopamine Microfluidic System toward a Two-Dimensional, Gravity-Driven Mixing Device. *Angew. Chem., Int. Ed.* **2012**, *51* (25), 6126−6130.
(11) Kim, J. S.; Kim, T. G.; Kong, W. H.; Park, T. G.; Nam, Y. S. Thermally Controlled Wettability of a Nanoporous Membrane Grafted with Catechol-Tethered Poly(N-Isopropylacrylamide). *Chem. Commun.* **2012**, *48* (74), 9227−9229.
(12) Park, J. Y.; Yeom, J.; Kim, J. S.; Lee, M.; Lee, H.; Nam, Y. S. Cell-Repellant Dextran Coatings of Porous Titania Using Mussel Adhesion Chemistry. *Macromol. Biosci.* **2013**, *13* (11), 1511−1519.
(13) Kim, I.; Son, H. Y.; Yang, M. Y.; Nam, Y. S. Bioinspired Design of an Immobilization Interface for Highly Stable, Recyclable Nanosized Catalysts. *ACS Appl. Mater. Interfaces* **2015**, *7* (26), 14415−14422.
(14) Hong, C. A.; Son, H. Y.; Nam, Y. S. Layer-by-Layer SiRNA/Poly(L-Lysine) Multilayers on Polydopamine-Coated Surface for Efficient Cell Adhesion and Gene Silencing. *Sci. Rep.* **2018**, *8* (1), 7738.
(15) Lee, K.; Oh, M. H.; Lee, M. S.; Nam, Y. S.; Park, T. G.; Jeong, J. H. Stabilized Calcium Phosphate Nano-Aggregates Using a Dopa-Chitosan Conjugate for Gene Delivery. *Int. J. Pharm.* **2013**, *445* (1−2), 196−202.
(16) Park, J. Y.; Kim, J. S.; Nam, Y. S. Mussel-Inspired Modification of Dextran for Protein-Resistant Coatings of Titanium Oxide. *Carbohydr. Polym.* **2013**, *97* (2), 753−757.
(17) Son, H. Y.; Kim, I.; Nam, Y. S. On-Surface Synthesis of Metal Nanostructures on Solid and Hydrated Polymer Nanofibers Coated with Polydopamine. *J. Ind. Eng. Chem.* **2015**, *30*, 220−224.
(18) Son, H. Y.; Kim, K. R.; Lee, J. B.; Le Kim, T. H.; Jang, J.; Kim, S. J.; Yoon, M. S.; Kim, J. W.; Nam, Y. S. Bioinspired Synthesis of Mesoporous Gold-Silica Hybrid Microspheres as Recyclable Colloidal SERS Substrates. *Sci. Rep.* **2017**, *7* (1), 14728.
(19) Sileika, T. S.; Barrett, D. G.; Zhang, R.; Lau, K. H. A.; Messersmith, P. B. Colorless Multifunctional Coatings Inspired by Polyphenols Found in Tea, Chocolate, and Wine. *Angew. Chem., Int. Ed.* **2013**, *52* (41), 10766−10770.
(20) Son, H. Y.; Ryu, J. H.; Lee, H.; Nam, Y. S. Silver-Polydopamine Hybrid Coatings of Electrospun Poly(Vinyl Alcohol) Nanofibers. *Macromol. Mater. Eng.* **2013**, *298* (5), 547−554.
(21) Son, H. Y.; Ryu, J. H.; Lee, H.; Nam, Y. S. Bioinspired Templating Synthesis of Metal-Polymer Hybrid Nanostructures within 3D Electrospun Nanofibers. *ACS Appl. Mater. Interfaces* **2013**, *5* (13), 6381−6390.
(22) Son, H. Y.; Lee, D. J.; Lee, J. B.; Park, C. H.; Seo, M.; Jang, J.; Kim, S. J.; Yoon, M. S.; Nam, Y. S. In Situ Functionalization of Highly Porous Polymer Microspheres with Silver Nanoparticles via Bio-Inspired Chemistry. *RSC Adv.* **2014**, *4* (98), 55604−55609.
(23) Son, H. Y.; Jun, H.; Kim, K. R.; Hong, C. A.; Nam, Y. S. Tannin-Mediated Assembly of Gold−Titanium Oxide Hybrid Nanoparticles for Plasmonic Photochemical Applications. *J. Ind. Eng. Chem.* **2018**, *63*, 420−425.
(24) Son, H. Y.; Kim, K. R.; Hong, C. A.; Nam, Y. S. Morphological Evolution of Gold Nanoparticles into Nanodendrites Using Catechol-Grafted Polymer Templates. *ACS Omega* **2018**, *3* (6), 6683−6691.
(25) Ahmad, T. Reviewing the Tannic Acid Mediated Synthesis of Metal Nanoparticles. *J. Nanotechnol.* **2014**, *2014*, 1−11.
(26) Huang, X.; Wang, Y.; Liao, X.; Shi, B. Adsorptive Recovery of Au^{3+} from Aqueous Solutions Using Bayberry Tannin-Immobilized Mesoporous Silica. *J. Hazard. Mater.* **2010**, *183* (1−3), 793−798.
(27) Gurung, M.; Adhikari, B. B.; Kawakita, H.; Ohto, K.; Inoue, K.; Alam, S. Recovery of Au(III) by Using Low Cost Adsorbent Prepared from Persimmon Tannin Extract. *Chem. Eng. J.* **2011**, *174* (2−3), 556−563.
(28) Adhikari, B. B.; Gurung, M.; Alam, S.; Tolnai, B.; Inoue, K. Kraft Mill Lignin - A Potential Source of Bio-Adsorbents for Gold Recovery from Acidic Chloride Solution. *Chem. Eng. J.* **2013**, *231*, 190−197.
(29) Wan, H.; Zou, Q.; Yan, R.; Zhao, F.; Zeng, B. Electrochemistry and Voltammetric Determination of Tannic Acid on a Single-Wall Carbon Nanotube-Coated Glassy Carbon Electrode. *Microchim. Acta* **2007**, *159* (1−2), 109−115.
(30) Wen, X.; Yang, S. Cu_2S/Au Core/Sheath Nanowires Prepared by a Simple Redox Deposition Method. *Nano Lett.* **2002**, *2* (5), 451−454.
(31) Hong, S.; Shuford, K. L.; Park, S. Shape Transformation of Gold Nanoplates and Their Surface Plasmon Characterization: Triangular to Hexagonal Nanoplates. *Chem. Mater.* **2011**, *23* (8), 2011−2013.
(32) Son, H. Y.; Koo, B. Il; Lee, J. B.; Kim, K. R.; Kim, W.; Jang, J.; Yoon, M. S.; Cho, J. W.; Nam, Y. S. Tannin-Titanium Oxide Multilayer as a Photochemically Suppressed Ultraviolet Filter. *ACS Appl. Mater. Interfaces* **2018**, *10* (32), 27344−27354.

DOI: 10.1021/acsami.9b05197
ACS Appl. Mater. Interfaces 2019, 11, 21915−21925

(33) Quici, N.; Litter, M. I.; Braun, A. M.; Oliveros, E. Vacuum-UV-Photolysis of Aqueous Solutions of Citric and Gallic Acids. *J. Photochem. Photobiol., A* **2008**, *197* (2−3), 306−312.
(34) Chang, T. C.; Chang, H. T.; Wu, C. L.; Lin, H. Y.; Chang, S. T. Stabilizing Effect of Extractives on the Photo-Oxidation of Acacia Confusa Wood. *Polym. Degrad. Stab.* **2010**, *95* (9), 1518−1522.
(35) Tennakone, K.; Kumara, G. R. R. A.; Kumarasinghe, A. R.; Sirimanne, P. M.; Wijayantha, K. G. U. Efficient Photosensitization of Nanocrystalline TiO_2 Films by Tannins and Related Phenolic Substances. *J. Photochem. Photobiol., A* **1996**, *94*, 217−220.
(36) Çakar, S.; Güy, N.; Özacar, M.; Findik, F. Investigation of Vegetable Tannins and Their Iron Complex Dyes for Dye Sensitized Solar Cell Applications. *Electrochim. Acta* **2016**, *209*, 407−422.
(37) McGilvray, K. L.; Granger, J.; Correia, M.; Banks, J. T.; Scaiano, J. C. Opportunistic Use of Tetrachloroaurate Photolysis in the Generation of Reductive Species for the Production of Gold Nanostructures. *Phys. Chem. Chem. Phys.* **2011**, *13* (25), 11914−11918.
(38) Narang, P.; Sundararaman, R.; Atwater, H. A. Plasmonic Hot Carrier Dynamics in Solid-State and Chemical Systems for Energy Conversion. *Nanophotonics* **2016**, *5* (1), 96−111.
(39) Lee, J. B.; Choi, S.; Kim, J.; Nam, Y. S. Plasmonically-Assisted Nanoarchitectures for Solar Water Splitting: Obstacles and Breakthroughs. *Nano Today* **2017**, *16*, 61−81.
(40) Brongersma, M. L.; Halas, N. J.; Nordlander, P. Plasmon-Induced Hot Carrier Science and Technology. *Nat. Nanotechnol.* **2015**, *10* (1), 25−34.
(41) Kim, J.; Son, H. Y.; Nam, Y. S. Multilayered Plasmonic Heterostructure of Gold and Titania Nanoparticles for Solar Fuel Production. *Sci. Rep.* **2018**, *8* (1), 10464.
(42) Choi, S.; Nam, Y. S. Gold−Titanium Dioxide Half-Dome Heterostructures for Plasmonic Hydrogen Evolution. *ACS Appl. Energy Mater.* **2018**, *15*, 39.
(43) Zhai, Y.; DuChene, J. S.; Wang, Y.-C.; Qiu, J.; Johnston-Peck, A. C.; You, B.; Guo, W.; DiCiaccio, B.; Qian, K.; Zhao, E. W.; Ooi, F.; Hu, D.; Su, D.; Stach, E. A.; Zhu, Z.; Wei, D. W. Polyvinylpyrrolidone-Induced Anisotropic Growth of Gold Nanoprisms in Plasmon-Driven Synthesis. *Nat. Mater.* **2016**, *15* (8), 889−895.
(44) Xue, C.; Millstone, J. E.; Li, S.; Mirkin, C. A. Plasmon-Driven Synthesis of Triangular Core-Shell Nanoprisms from Gold Seeds. *Angew. Chem., Int. Ed.* **2007**, *46* (44), 8436−8439.
(45) Jin, R.; Cao, Y. C.; Hao, E.; Métraux, G. S.; Schatz, G. C.; Mirkin, C. A. Controlling Anisotropic Nanoparticle Growth through Plasmon Excitation. *Nature* **2003**, *425* (6957), 487−490.
(46) Jin, R.; Cao, Y.; Mirkin, C. A.; Kelly, K. L.; Schatz, G. C.; Zheng, J. G. Photoinduced Conversion of Silver Nanospheres to Nanoprisms. *Science* **2001**, *294* (5548), 1901−1903.
(47) Kim, J. W.; Lee, J. E.; Ryu, J. H.; Lee, J. S.; Kim, S. J.; Han, S. H.; Chang, I. S.; Kang, H. H.; Suh, K. Do. Synthesis of Metal/Polymer Colloidal Composites by the Tailored Deposition of Silver onto Porous Polymer Microspheres. *J. Polym. Sci., Part A: Polym. Chem.* **2004**, *42* (10), 2551−2557.
(48) Kim, Y. J.; Kim, J. W.; Lee, J. E.; Ryu, J. H.; Kim, J.; Chang, I. S.; Suh, K. Do. Synthesis and Adsorption Properties of Gold Nanoparticles within Pores of Surface-Functional Porous Polymer Microspheres. *J. Polym. Sci., Part A: Polym. Chem.* **2004**, *42* (22), 5627−5635.
(49) Rudzinski, W.; Plazinski, W. Kinetics of Solute Adsorption at Solid/Solution Interfaces: A Theoretical Development of the Empirical Pseudo-First and Pseudo-Second Order Kinetic Rate Equations, Based on Applying the Statistical Rate Theory of Interfacial Transport. *J. Phys. Chem. B* **2006**, *110* (33), 16514−16525.
(50) Liu, Y.; Shen, L. From Langmuir Kinetics to First- and Second-Order Rate Equations for Adsorption. *Langmuir* **2008**, *24* (20), 11625−11630.
(51) Foo, K. Y.; Hameed, B. H. Insights into the Modeling of Adsorption Isotherm Systems. *Chem. Eng. J.* **2010**, *156* (1), 2−10.
(52) Ranoszek-Soliwoda, K.; Tomaszewska, E.; Socha, E.; Krzyczmonik, P.; Ignaczak, A.; Orlowski, P.; Krzyzowska, M.; Celichowski, G.; Grobelny, J. The Role of Tannic Acid and Sodium Citrate in the Synthesis of Silver Nanoparticles. *J. Nanopart. Res.* **2017**, *19* (8), 273.
(53) Sundarapandiyan, S.; Renitha, T. S.; Sridevi, J.; Chandrasekaran, B.; Saravanan, P.; Raju, G. B. Mechanistic Insight into Active Chlorine Species Mediated Electrochemical Degradation of Recalcitrant Phenolic Polymers. *RSC Adv.* **2014**, *4* (104), 59821−59830.
(54) Leenheer, A. J.; Narang, P.; Lewis, N. S.; Atwater, H. A. Solar Energy Conversion via Hot Electron Internal Photoemission in Metallic Nanostructures: Efficiency Estimates. *J. Appl. Phys.* **2014**, *115*, 134301.
(55) Patil, N.; Jérôme, C.; Detrembleur, C. Recent Advances in the Synthesis of Catechol-Derived (Bio)Polymers for Applications in Energy Storage and Environment. *Prog. Polym. Sci.* **2018**, *82*, 34−91.
(56) Novak, I.; Šeruga, M.; Komorsky-Lovrić, Š. Electrochemical Characterization of Epigallocatechin Gallate Using Square-Wave Voltammetry. *Electroanalysis* **2009**, *21* (9), 1019−1025.
(57) Guin, P. S.; Das, S.; Mandal, P. C. Electrochemical Reduction of Quinones in Different Media: A Review. *Int. J. Electrochem.* **2011**, *2011*, 1−22.
(58) Harada, M.; Einaga, H. In Situ XAFS Studies of Au Particle Formation by Photoreduction in Polymer Solutions. *Langmuir* **2007**, *23* (12), 6536−6543.
(59) Wu, Z.; Yuan, W.; Li, J.; Wang, X.; Liu, L.; Wang, J. A Critical Review on the Recycling of Copper and Precious Metals from Waste Printed Circuit Boards Using Hydrometallurgy. *Front. Environ. Sci. Eng.* **2017**, *11* (5), 8.
(60) Yamane, L. H.; de Moraes, V. T.; Espinosa, D. C. R.; Tenório, J. A. S. Recycling of WEEE: Characterization of Spent Printed Circuit Boards from Mobile Phones and Computers. *Waste Manage.* **2011**, *31* (12), 2553−2558.
(61) Jha, M. K.; Lee, J.; Kim, M.; Jeong, J.; Kim, B.-S.; Kumar, V. Hydrometallurgical Recovery/Recycling of Platinum by the Leaching of Spent Catalysts: A Review. *Hydrometallurgy* **2013**, *133*, 23−32.
(62) Iglesias, M.; Antico, E.; Salvado, V. Recovery of Palladium (II) and Gold (III) from Diluted Liquors Using the Resin Duolite GT-73. *Anal. Chim. Acta* **1999**, *381*, 61−67.
(63) Yong, P.; Rowson, N. A.; Farr, J. P. G.; Harris, I. R.; Macaskie, L. E. Bioaccumulation of Palladium by Desulfovibrio Desulfuricans. *J. Chem. Technol. Biotechnol.* **2002**, *77* (5), 593−601.
(64) Kvítek, L.; Prucek, R.; Panáček, A.; Novotný, R.; Hrbáč, J.; Zbořil, R. The Influence of Complexing Agent Concentration on Particle Size in the Process of SERS Active Silver Colloid Synthesis. *J. Mater. Chem.* **2005**, *15* (10), 1099−1105.
(65) Harris, D. C.. *Quantitative Chemical Analysis*, Seventh Ed.; W.H. Freeman and Company: New York, 2007; Vol. *1*. DOI: 10.1017/CBO9781107415324.004.
(66) Meena Kumari, M.; Aromal, S. A.; Philip, D. Synthesis of Monodispersed Palladium Nanoparticles Using Tannic Acid and Its Optical Non-Linearity. *Spectrochim. Acta, Part A* **2013**, *103*, 130−133.
(67) Mondal, M.; Begum, T.; Gogoi, P. K.; Bora, U. Gallic Acid Derived Palladium(0) Nanoparticles: An In Situ Formed "Green and Recyclable" Catalyst for Suzuki-Miyaura Coupling in Water. *ChemistrySelect* **2016**, *1* (15), 4645−4651.
(68) Guo, J.; Ping, Y.; Ejima, H.; Alt, K.; Meissner, M.; Richardson, J. J.; Yan, Y.; Peter, K.; Von Elverfeldt, D.; Hagemeyer, C. E.; Caruso, F. Engineering Multifunctional Capsules through the Assembly of Metal-Phenolic Networks. *Angew. Chem., Int. Ed.* **2014**, *53* (22), 5546−5551.

DOI: 10.1021/acsami.9b05197
ACS Appl. Mater. Interfaces 2019, 11, 21915−21925